

Coherent oscillations and the evolution of the emission area in the decaying phase of radius-expansion bursts from 4U 1636–53

Guobao Zhang^{1*}, Mariano Méndez¹, Tomaso M. Belloni², and Jeroen Homan³

¹*Kapteyn Astronomical Institute, University of Groningen, P.O. BOX 800, 9700 AV Groningen, The Netherlands*

²*INAF – Osservatorio Astronomico di Brera, Via E. Bianchi 46, I-23807 Merate (LC), Italy*

³*MIT Kavli Institute for Astrophysics and Space Research, 70 Vassar Street, Cambridge, MA 02139, USA*

2 March 2013

ABSTRACT

We analyzed all archival data of the low-mass X-ray binary system 4U 1636–53 with the Rossi X-ray Timing Explorer (1490 observations). We found a total of 336 type-I X-ray bursts from this source. From fits to the time-resolved spectra, we classified 69 of these bursts as photospheric radius-expansion (PRE) bursts. PRE bursts show a characteristic time profile in which the fitted blackbody radius increases rapidly at the beginning of the burst, and then drops abruptly close to the peak of the burst. The lowest value of the radius after the expansion phase defines the so-called touchdown point. We found that in 17 of the PRE bursts, after the touchdown point, the blackbody radius increases again quickly after about 1 second, and from then on the radius decreases slightly or it remains more or less constant. In the other 52 PRE bursts, after touchdown, the radius of the blackbody stays more or less constant for $\sim 2 - 8$ seconds, and after that it increases slowly. Interestingly, those PRE bursts in which the blackbody radius remains more or less constant for ≥ 2 seconds show coherent oscillations in the tail of the burst, whereas those PRE in which the blackbody radius changes rapidly after touchdown show no coherent oscillations in the tail of the burst. From a Kolmogorov-Smirnov test we find that the difference between the two groups of PRE bursts is significant at a $5-\sigma$ level. This is the first time that the presence of burst oscillations in the tail of X-ray bursts is associated with a systematic behaviour of the spectral parameters in that phase of the bursts. This result is consistent with predictions of models that associate the oscillations in the tail of X-ray bursts with the propagation of a cooling wake in the material on the neutron-star surface during the decay of the bursts.

Key words: stars: neutron — X-rays: binaries — X-rays: bursts — stars: individual: 4U 1636–53

1 INTRODUCTION

Thermonuclear, type-I, X-ray bursts (e.g., Lewin et al. 1993; Strohmayer & Bildsten 2003; Galloway et al. 2008) are due to unstable burning of H and He on the surface of accreting neutron stars in low-mass X-ray binaries (LMXBs). Some X-ray bursts are strong enough to lift up the outer layers of the star. During these so-called photospheric radius expansion (PRE) bursts (e.g., Basinska et al. 1984; Kuulkers et al. 2002), the radiation flux that emerges from the stellar surface is limited by the Eddington flux.

One of the best studied sources of X-ray bursts is the LMXB 4U 1636–53. For instance, from observations with the Rossi X-ray Timing Explorer (RXTE) up to May 2010, Zhang et al. (2011) detected 298 X-ray bursts. Most of these bursts have standard, single-peaked, fast rising and exponentially decaying light curves; 52 of these bursts are PRE bursts (Zhang et al. 2011).

Some of the bursts in 4U 1636–53 show millisecond oscillations at 581 Hz, the so-called burst oscillations (Strohmayer et al. 1998). This oscillations likely reflect the spin frequency of the neutron star (Strohmayer et al. 1997; Chakrabarty et al. 2003). Similar burst oscillations have been detected in several other low-luminosity accreting neutron-star systems (for a review see, e.g. Munro et al.

* E-mail: zhang@astro.rug.nl

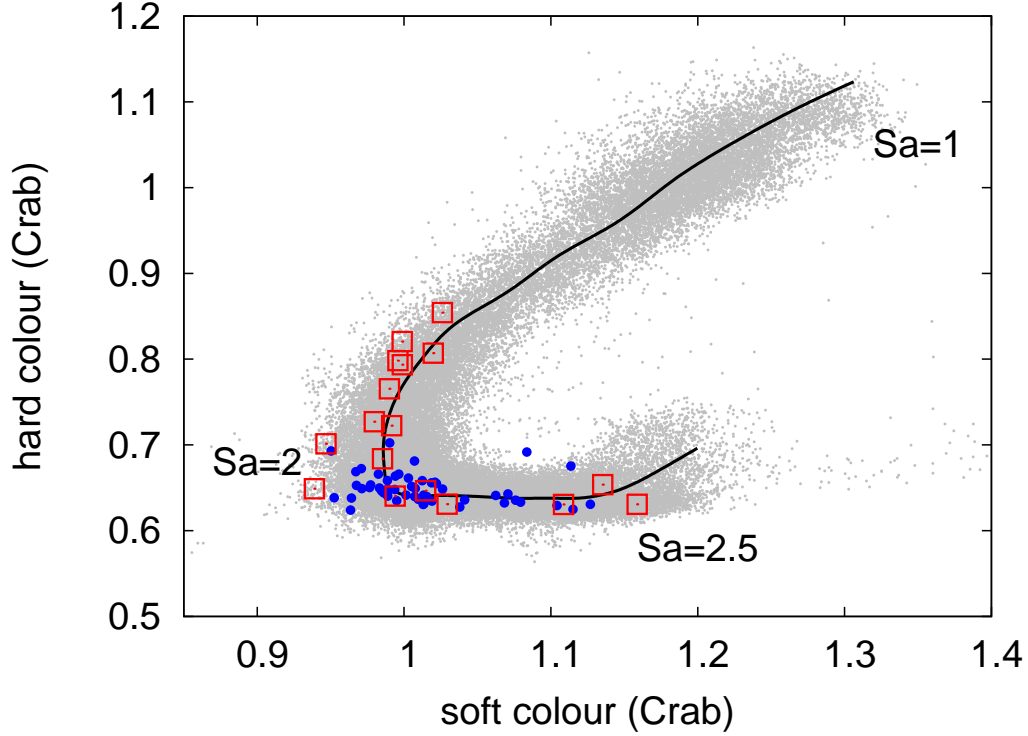


Figure 1. Colour-colour diagram of all RXTE observations of 4U 1636–53. The grey points represent the colours of the source from all available RXTE observations. Each point in this diagram corresponds to 256 s of data. The colours of 4U 1636–53 are normalized to the colours of Crab. The blue filled circles represent the colours of the persistent emission of the source at the onset of a PRE X-ray burst with tail oscillations. The red open squares indicate the same for PRE bursts without tail oscillations. The position of the source on the diagram is parametrized by the length of the black solid curve S_a .

2001), e.g. 4U 1728–34, 4U 1608–52, KS 1731–260 and Aquila X–1. Burst oscillations do not occur in every burst from these LMXBs; but when burst oscillations are present, they occur sometimes during the rise, sometimes in the decay, and sometimes both in the rise and the decay of the burst. In KS 1731–260, oscillations are only found at high mass accretion rate, both in the rise and the decay of the burst, and all but one of the bursts with oscillations also show radius expansion (Muno et al. 2001). In 4U 1728–34, burst oscillations (both in the rise and the decay) are also only detected when the mass accretion rate is high, whereas most PRE bursts occur when the accretion rate is low, and these PRE bursts show no burst oscillations (van Straaten et al. 2001; Franco 2001). In 4U 1636–53, the situation is more complex than in 4U 1731–260 and 4U 1728–34. Burst oscillations in 4U 1636–53 are observed both in PRE and non-PRE bursts, and are detected both at low and high mass accretion rate (Zhang et al. 2011). From these results, it appears that in 4U 1636–53 burst oscillations are neither correlated with mass accretion rate nor with the PRE phenomenon.

Burst oscillations have been explained as arising from rotation of a brightness asymmetry on the neutron-star surface at the spin frequency of the neutron star (Strohmayer et al. 1997). Asymmetries in the emission pattern of the neutron-star surface in the rising phase of thermonuclear X-ray bursts can be due to initially localized nuclear burning at the place where the burst first ignites; the flame front subsequently spreads to the entire neutron-star

surface, and the asymmetry, and hence the oscillations, disappears (Strohmayer et al. 1996). Strohmayer et al. (1997) found that the amplitude of the burst oscillations in 4U 1728–34 decreases monotonically as the burst flux increases during the rising phase of the burst. This result is consistent with the spreading hotspot model, since as the spot grows in size, the amplitude of the oscillation should decrease.

As we already mentioned, oscillations are detected not only in the rising, but also at the peak and the decaying phase (the so-called tail) of X-ray burst; in fact, burst oscillations are most commonly detected in the tail of the bursts (hereafter tail oscillations; van Straaten et al. 2001; Muno et al. 2002; Galloway et al. 2008). Most burst oscillations exhibit a frequency drift of $\sim 1 - 5$ Hz in the tail of the burst (Wijnands 2001; Galloway et al. 2001; Muno et al. 2002). In general the frequency of the oscillations increases towards an asymptotic value in the tail of the burst, although Strohmayer et al. (1998) and Strohmayer (1999) found that in 4U 1636–53 the frequency of the oscillations decreases in some bursts. The spreading hotspot model can neither explain the tail oscillations, nor this frequency drift (Cumming & Bildsten 2000; Cumming et al. 2002).

Regarding the tail oscillations, Payne & Melatos (2006) proposed that during the decaying phase of the burst, the burning front is stalled by the presence of a magnetic field; the combination of partial surface burning and magnetic fields could lead to anisotropic emission during the tail of X-ray bursts. Alternatively, a cooling wake in the tail of the burst due to hydrodynamic instabilities can also

produce asymmetric emission (Spitkovsky et al. 2002). Finally, instability modes (eg., pressure, gravity, buoyancy, etc.) excited in the neutron star burning layer can also produce burst oscillations; this scenario can also account for the observed frequency drift of the oscillations in the tail of some bursts (Cumming & Bildsten 2000; Heyl 2004; Piro & Bildsten 2005).

In this paper we compare simultaneous power density spectra and time-resolved energy spectra of 336 X-ray bursts in 4U 1636–53. We find that bursts with oscillations in the tail of the burst always show an extended period of a more or less constant blackbody radius during the burst decay. We describe the observations and data analysis in §2, and we present our results in §3. Finally, in §4 we discuss our findings and compare them with current models for burst oscillations.

2 OBSERVATION AND DATA ANALYSIS

We analyzed all available data (1490 observations) of 4U 1636–53 from the Proportional Counter Array (PCA) on board RXTE. The PCA consists of an array of five collimated proportional counter units (PCUs) operating in the 2–60 keV range. We produced 0.5-s light curves from the Standard-1 data (0.125-s time-resolution with no energy resolution) and searched for X-ray bursts in these light curves following the procedure described in Zhang et al. (2011).

We used the Standard-2 data (16-s time-resolution and 129 channels covering the full 2 – 60 keV PCA band) to calculate X-ray colours of the source (see Zhang et al. 2011, for details). Hard and soft colours are defined as the 9.7 – 16.0/6.0 – 9.7 keV and 3.5 – 6.0/2.0 – 3.5 keV count rate ratios, respectively. We show the colour-colour diagram (CCD) of all observations of 4U 1636–53 in Figure 1. We parametrized the position of the source on the diagram by the length of the solid curve S_a (see, e.g. Méndez et al. 1999), fixing the values of $S_a = 1$ and $S_a = 2$ at the top-right and the bottom-left vertex of the CCD, respectively.

In order to study the bursts in detail, we used the high-time resolution modes that were available for each observation to produce time-resolved spectra of each burst. About 8% of the observations have a mode with 500- μ s time resolution. The rest of the observations have a mode with at least 125- μ s time resolution. For every burst we produced a spectrum every 0.25 s during the rising part and the peak, and 0.5 s, 1 s and 2 s during the decay, covering the whole duration of the burst. The variable exposure time was tailored to collect more or less the same number of counts per spectrum. We generated the instrument response matrix for each spectrum with the standard FTOOLS routine *pcarsp*, and we corrected each spectrum for dead time using the methods supplied by the RXTE team. Because of the short exposure of each spectrum, in this case the statistical errors dominate, and therefore we did not add any systematic error to the spectra. For each burst we extracted the spectrum of the persistent emission just before (or after) the burst to use as background in our fits; this approach, used to obtain the net emission of a burst, is a well established procedure in X-ray burst analysis (e.g. Kuulkers et al. 2002). We note that this procedure fails if the blackbody component during the burst comes from the same source that produces the black-

body component seen in the persistent emission, since the difference between two blackbody spectra is not a blackbody (van Paradijs & Lewin 1986). This effect is significant only when the net burst emission is small, and therefore problems may arise only at the start and the tail of the burst, when the burst emission is comparable to the persistent emission (see the discussion in Kuulkers et al. 2002). In Zhang et al. (2011), we already established that this issue does not affect the spectral results in 4U 1636–53.

We fitted the spectra using XSPEC version 12.7.0 (Arnaud 1996), restricting the spectral fits to the energy range 3.0 – 20.0 keV. We fitted the time-resolved net burst spectra with a single-temperature blackbody model (*bbbodyrad* in XSPEC), as generally burst spectra are well fitted by a blackbody (Galloway et al. 2008). We also included the effect of interstellar absorption along the line of sight using the XSPEC model *wabs*. During the fitting we kept the hydrogen column density, N_H , fixed at $0.36 \times 10^{22} \text{cm}^{-2}$ (Pandel et al. 2008), and to calculate the radius of the emitting blackbody area in km, R_{bb} , we assumed a distance of 5.95 kpc (Galloway et al. 2008).

For each burst we computed Fourier power density spectra (PDS) from 2-s data segments for the duration of the burst using the data over the full PCA band pass, setting the start time of each segment to 0.125 s after the start time of the previous segment. Because of this, the individual power spectra are not independent. The Nyquist frequency of these power spectra was always 1024 Hz. We used these PDS to produce time-frequency plots (also known as dynamic power spectra; see Berger et al. 1996) of each burst. For each burst, we searched for coherent oscillations between 577 Hz and 582 Hz for the duration of the burst. We considered that a signal was significant if it had a probability of $< 10^{-4}$ that it was produced by noise, accounting for the number of independent trials. Since the individual power spectra are not independent, to estimate the number of trials we divided the duration of the burst by the length of the PDS (2 s). Finally, we consider that a burst has tail oscillations if the oscillations appear after the peak of the burst. If we normalize the power spectra according to Leahy et al. (1983), the fractional rms amplitude at a given frequency is

$$A = \left(\frac{P_m}{I_\gamma} \right)^{\frac{1}{2}} \left(\frac{I_\gamma}{I_\gamma - I_b} \right), \quad (1)$$

where P_m is the measured power, I_γ is the total number of counts (source plus background), and I_b is the number of background counts (Belloni & Hasinger 1990). To calculate the signal power, P_s , from the measured power, and accounting for the distribution of powers from Poisson noise in the power spectrum, we used the algorithm described in the appendix of Vaughan et al. (1994). We calculated the error bars of the rms amplitude using the same method discussed in Watts et al. (2005). For details on how to calculate the signal power from the measured power, see Vaughan et al. (1994), Munro et al. (2002), Watts et al. (2005) and Watts (2012).

3 RESULTS

We examined the time-resolved energy spectra of all the 336 bursts in 4U 1636–53 to identify the PRE and non-PRE

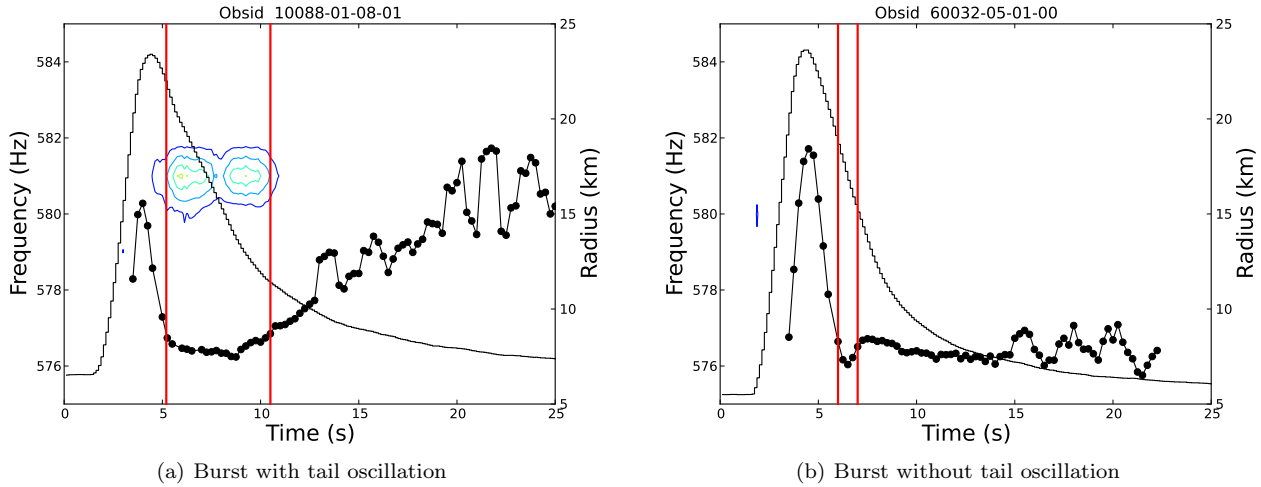


Figure 2. Left panel: A PRE burst with tail oscillation. Right panel: A PRE burst without tail oscillations. The black histogram shows the average count rate in 2-s interval every 0.125s. The contour lines show constant power values, increasing from 10 to 40 in steps of 10 (values are in Leahy units), as a function of frequency (see the left y-axis). Black filled circles connected by a line show the blackbody radius as a function of time (see the right y-axis). The red vertical lines define the PTD phase (see text). Note also the power contours at $\sim 579 - 581$ Hz at the beginning of the bursts, which are due to oscillations in the rising of the burst.

bursts. Here we concentrate only on the PRE bursts, and in particular in the time interval immediately after the radius expansion and contraction phase. In all PRE bursts the blackbody radius first increases, it then decreases abruptly to a local minimum (the so-called touch-down, TD, point) and after that it either increases or decreases slowly. We show two examples of PRE bursts in Figure 2. In order to compare the power spectrum and the fitted blackbody radius within the same time interval, we first fitted the energy spectrum every 0.25 s, and we then calculated the average blackbody radius in 2-s interval (8 consecutive energy spectra). We plot the average blackbody radius as a function of time with black filled circles connected with a line in Figure 2. We also show the burst light curve at a resolution of 2 s and a 0.125-s step with the solid line in that Figure.

We find that the behaviour of the blackbody radius after TD is not the same in all PRE bursts. In 52 out of the 69 PRE bursts, after the expansion phase the blackbody radius first decreases rapidly, it then continues decreasing at a lower rate, it reaches a minimum value of $\sim 7 - 8$ km, and finally it increases slowly towards the tail of the burst (see Figure 2(a)). In the other 17 PRE bursts, after the expansion phase the blackbody radius first decreases rapidly to a minimum of $\sim 7 - 8$ km, then it immediately increases again very quickly, and finally it either decreases slightly, or it remains more or less constant (see Figure 2(b)). We can classify all 69 PRE bursts in 4U 1636–53 into one of these two groups.

While it is apparent that the duration of the phase around the minimum radius is not always the same among the 69 PRE bursts, we need to find an objective way to measure the length of this phase, for instance choosing a contiguous time interval within which the radius is below a certain value. Clearly this value has to be larger than the minimum radius reached in all bursts after the expansion phase, and it has to be smaller than the local maximum of the radius just after the radius at the touchdown point in bursts like the one in Figure 2(b). We therefore define

the post touchdown (PTD) phase as the contiguous time interval after the peak of the burst in which the radius of the fitted blackbody is less than 8 km. Our results do not change significantly if we choose a value between 8 km and 8.5 km. If we used a value smaller than 8 km, the length of the PTD phase of several bursts would be zero, while if we used a value larger than 8.5 km, the length of the PTD phase of several bursts would be unbound. We indicate the PTD phase by the two red vertical lines in Figure 2. We find that most PRE bursts in 4U 1636–53 show a long PTD phase, $t_{\text{PTD}} > 2 - 8$ s.

We also examined all the dynamic power spectra of these PRE bursts, concentrating only on the oscillations in the decaying phase of the burst. We find that 52 out of the 69 PRE bursts in 4U 1636–53 have tail oscillations (see contour plot in Figure 2(a)). The contours of constant power as a function of frequency and time shown in Figure 2(a) were calculated from 2-s power spectra. We calculated the upper limit of the power for the 17 PRE bursts in which we did not detect tail oscillations (Groth 1975; Vaughan et al. 1994). Except for four bursts, the upper limits are lower than the average power of the detected tail oscillations. During the other four bursts only one or two of the five PCU detectors were on, and hence the upper limits are not very constraining. From the two examples in Figure 2 it is apparent that the burst in Figure 2(a), which shows a long (~ 6 s) PTD phase, has oscillations at the tail, while the burst in Figure 2(b), which has a short (~ 1 s) PTD phase, has no oscillations at the tail.

We find that bursts that show tail oscillations have in general longer PTD phase than those that do not show tail oscillations. In order to quantify this, we calculated the duration of the PTD phase, hereafter the PTD time, for all PRE bursts and divided the PRE bursts into two groups: burst with and without tail oscillations. Figure 3(a) shows the distribution of the time for PRE bursts with (blue thick lines) and without (green thin lines) tail oscillations. This plot con-

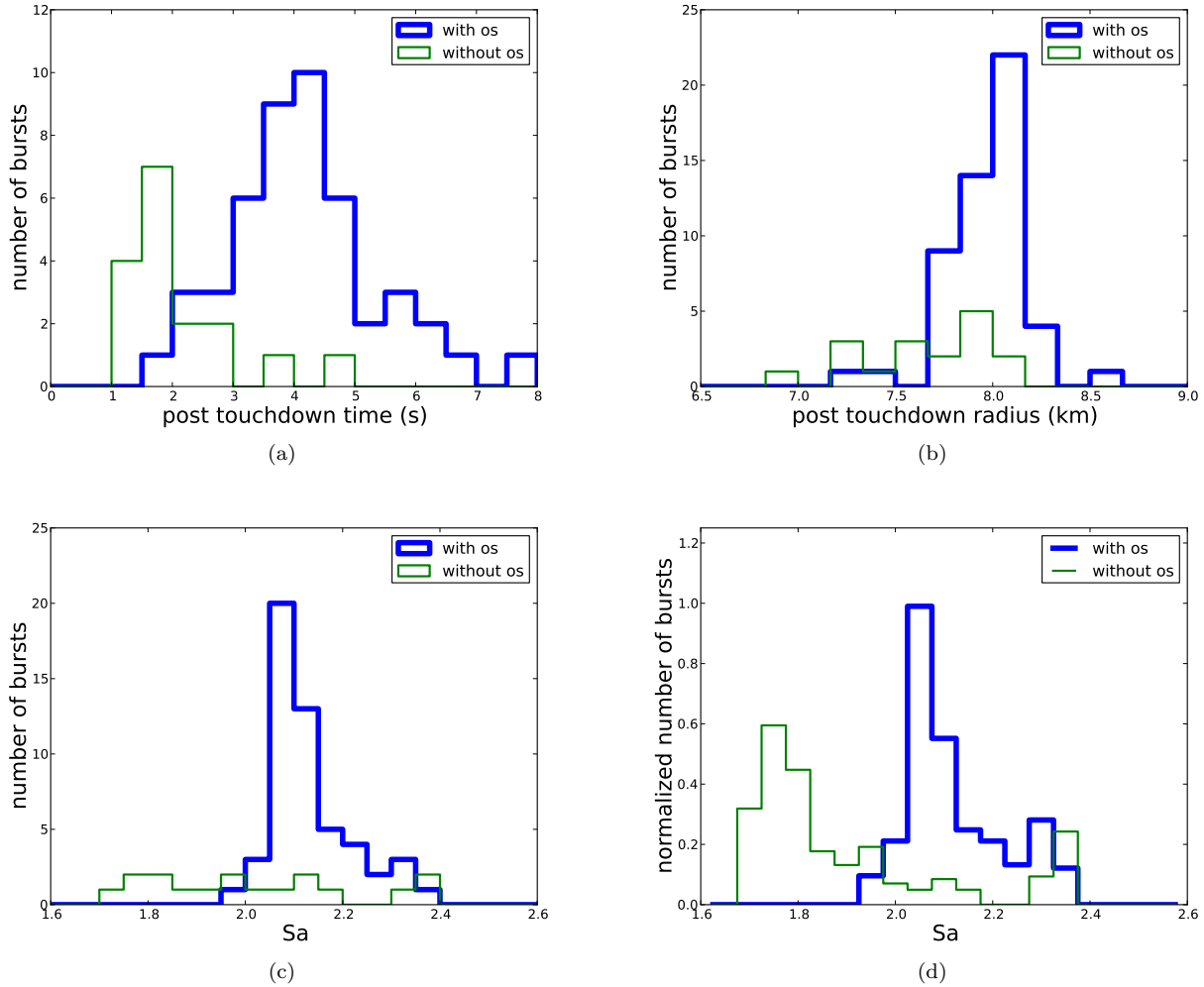


Figure 3. Top panel: Distribution of, respectively, the PTD time and average PTD radius for the PRE bursts with and without tail oscillations in 4U 1636–53. Bottom panel: Distribution of the S_a values for, respectively, the raw data and exposure-normalized bursts with and without tail oscillations in 4U 1636–53. The bursts with and without oscillations are shown by thick blue lines and thin green lines, respectively.

firmers our initial impression: bursts with tail oscillations have on average ~ 4 times longer PTD times than burst without tail oscillations. We carried out a Kolmogorov–Smirnov (KS) test to assess whether the two distributions are consistent with being samples of the same parent population. We find a chance probability of 3.5×10^{-7} .

We also calculated the average PTD blackbody radius (hereafter PTD radius) for PRE bursts with and without tail oscillations. The two distributions are plotted in Figure 3(b). The KS-test probability that both samples come from the same parent population is 2.2×10^{-3} .

Figure 3(c) shows the distributions of S_a for the PRE bursts with and without tail oscillations. We find that the PRE bursts with tail oscillations have S_a values that are larger than 1.9, and the distribution peaks at $S_a \sim 2.1$, whereas PRE bursts without tail oscillations distribute uniformly from $S_a \sim 1.7$ to $S_a \sim 2.4$,

To compensate for the fact that RXTE did not sample the CCD of 4U 1636–53 evenly, we normalized the bursts number per S_a bin in Figure 3(c) by the total exposure time

with RXTE at each position in the CCD. We show the resulting distribution in Figure 3(d). We find that the distribution of S_a in PRE bursts with tail oscillations still peaks at $S_a \sim 2.1$, whereas the distribution of S_a in PRE bursts without tail oscillations peaks at $S_a \sim 1.75$. The KS probability that the two S_a distributions¹ come from the same parent population is 4.4×10^{-4} .

In order to check whether there is a correlation between the PTD radius and the amplitude of the tail oscillation, for each burst we calculated the PTD radius and the rms amplitude of the tail oscillations every second and averaged the values for each burst. After that, we rebinned the data by a factor of 6 and plotted them in Figure 4. From this Figure it appears that the fractional rms amplitude decreases as the

¹ This is the KS probability from the raw data, i.e., without normalizing the number of bursts per S_a interval according to the RXTE exposure along the CCD. We get an even lower probability if we instead compare the two histograms in Figure 3(c) using the χ^2 test. Here we take the most conservative result.

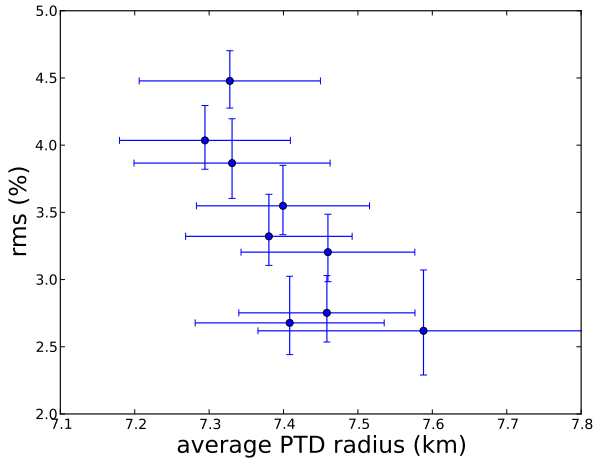


Figure 4. Fractional rms amplitude versus PTD radius for all the PRE bursts with tail oscillations in 4U 1636-53.

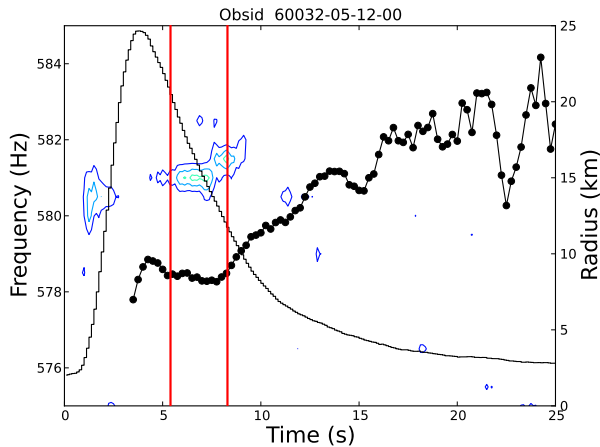


Figure 5. A non-PRE burst with tail oscillations in 4U 1636-53. The symbols are the same as in Figure 3.

average PTD radius increases. We fitted the data both with a constant and a linear function, and we carried out an F-test to compare both fits. The F-test probability is 6.1×10^{-3} , indicating that a linear fit is marginally better than a fit with a constant. We found no significant correlation between fractional rms amplitude and PTD time.

We also detected nine non-PRE bursts with tail oscillations in our observations. Similar to the case of PRE bursts, after the peak of the burst, the energy spectra of these non-PRE bursts show a period in which R_{bb} remains more or less constant during the time in which tail oscillations are present (see Figure 5). However, in this case it is difficult to identify the PTD phase because non-PRE bursts do not have (by definition) a radius expansion phase, and a subsequent TD point. We therefore did not include non-PRE bursts in our analysis, although it is quite possible that the connection between constant R_{bb} and tail oscillations applies also to this kind of bursts.

4 DISCUSSION

We analyzed all 336 type-I X-ray bursts in the LMXB 4U 1636-53 observed with RXTE; 69 of them are PRE bursts. For the first time, we correlated the behaviour of the spectral parameters of the bursts with the presence of oscillations in the decaying phase of these PRE bursts. We find that, after the radius contraction phase, in some bursts the blackbody radius reaches a minimum value followed by a fast increase (short PTD phase). We do not detect burst oscillations during the decaying phase of these bursts. In other bursts, the blackbody radius reaches the minimum value followed by a slow evolution (long PTD phase). We do detect tail oscillations in these bursts. We compare the PTD time in the PRE bursts with and without tail oscillations, and find a significant difference (5σ) between the two burst classes.

The mechanism that produces burst oscillations, and why these oscillations are not present in all type-I X-ray bursts, still remains unclear (Strohmayer et al. 1996, 1998; Munro et al. 2002; Munro 2004). Unstable nuclear burning is likely not happening uniformly across the neutron-star surface so, as the neutron star rotates, variations of the neutron-star surface brightness and the neutron-star rotation should produce oscillations during an X-ray burst. Strohmayer et al. (1996) suggested that burst oscillations are caused by asymmetries due to initially localized nuclear burning (the ignition point of the burst) that later spreads over the surface of the neutron star in the rising phase of the burst. This scenario, however, cannot explain the tail oscillations that persist for as long as 5–10 s, unless the asymmetry can be maintained for such a long period. Bildsten (1995) suggested that in some bursts only part of the surface is burning; magnetic fields and patchy burning could lead to anisotropic emission during X-ray bursts. Cumming & Bildsten (2000), Heyl (2004) and Piro & Bildsten (2005) proposed that modes (eg., pressure, gravity, buoyancy, etc.) excited in the neutron-star burning layer can produce burst oscillations in the tail of the burst, and that the frequency drift observed in the tail of some bursts is due to a changing mode frequency as the burning layer cools. Spitkovsky et al. (2002) suggested that the oscillations in the rising phase of the burst are from a slow-moving spot on the neutron-star surface. The brightness anisotropy may arise from hydrodynamic instabilities in the burning material. Spitkovsky et al. (2002) found that the speed of the burning front near the equator is higher than that near the poles. Furthermore, these authors also suggested that tail oscillations could be due to the spread of a cooling wake, which is formed by vortices during the cooling of the neutron-star atmosphere. In this scenario, the speed of the cooling wake would also depend on latitude. Cumming (2005) connected the ideas of unstable zonal flows and oscillation modes, and studied the linear stability of shearing zonal flows during the tail of type-I X-ray bursts. He found that a differential rotation of 2% between the pole and the equator, with the equator spinning faster than the poles, is unstable to hydrodynamic shear instabilities. Growth of shear instabilities may explain the brightness asymmetry that produces the oscillations in the tails of X-ray bursts.

Our results match some of the predictions of the model by Spitkovsky et al. (2002), if we assume that the bursts with tail oscillations are due to a cooling wake starting near

the poles, while bursts without tail oscillations are due to a cooling wake starting near the equator. According to this model, the width and speed of the cooling wake should decrease by a factor of ~ 4 as the front propagates from the equator to the pole. If the cooling wake starts from the equator, then the entire equator belt is likely covered very rapidly, and the asymmetry during the cooling, which is needed for the burst oscillations, disappears. After the atmosphere contracts to the neutron star surface, the emission area changes very quickly due to the high speed of the cooling wake near the equator. These bursts would then have no tail oscillations and a short PTD phase.

If the cooling wake starts at high latitude, the front speed is slower than that in the equator (see Fig. 8 in Spitkovsky et al. 2002). After the atmosphere contracts to the neutron-star surface, the emission area changes slowly. The low speed of the cooling wake on the neutron star means that the asymmetric emission during the tail of the burst lasts longer, and the emission area changes slowly. These bursts would then have tail oscillations and a long PTD phase. It is interesting that bursts with tail oscillations have a PTD time that is about 4 times longer than that of bursts without tail oscillations (see Figure 3(a)), consistent with the prediction of Spitkovsky et al. (2002).

Following the model by Spitkovsky et al. (2002), Cooper & Narayan (2007) found that in a neutron-star X-ray binary system, when the source evolves from low to high mass accretion rate, the area where physical conditions for unstable burning (where the burst should ignite) moves from low to high latitudes on the neutron-star surface. We find that PRE bursts with tail oscillations always appear in the colour-colour diagram at high S_a values (see histogram with thick lines in Figure 3(c)). S_a is considered to be correlated to mass accretion rate (Hasinger & van der Klis 1989; Méndez et al. 1999). This suggests that the cooling wake of PRE bursts with tail oscillations starts at high latitude, when the source is in the high mass accretion rate state.

If bursts oscillations are due to a brightness asymmetry on the neutron-star surface, the larger the area of the asymmetry the smaller the amplitude of the modulation. In Figure 4 we find marginal evidence that the fractional rms amplitude decreases as the average PTD radius increases in bursts with tail oscillations.

We note that the observed changes in the blackbody radius in the tail of X-ray bursts could also be due to the effect of spectral hardening (colour factor), caused by the electron scattering in the neutron star atmosphere (Suleimanov et al. 2011; Zhang et al. 2011). Since the colour factor depends mainly on the ratio L/L_{Edd} , and the PRE bursts in 4U 1636–53 always show similar flux during the PTD phase, the colour factor cannot explain the different duration of the PTD phase in the PRE bursts. Kaptein et al. (2000) tried to correct the temperature and radius in X-ray bursts for this effect, but changes in the blackbody radius do not disappear after applying this correction.

The reason to study the tail oscillations only in PRE bursts is that the phase after the TD point can only be identified in PRE bursts (since non-PRE bursts do not have a touchdown point). Nevertheless, the relation between PTD radius and PTD time on one hand, and tail oscillations on the other, may actually extend to non-PRE bursts as well. Some non-PRE bursts in 4U 1636–53 show tail oscillations,

and the blackbody radius stays constant as well during the oscillating time (see Figure 5). This suggests that tail oscillations are always associated with an emitting area that remains constant for a while, regardless of the nature (PRE or non-PRE) of the bursts. We note that there are instances in which the blackbody radius stays constant for a sufficiently long period in some non-PRE bursts in 4U 1636–53, whereas tail oscillations are not detected in these bursts. This suggests that the blackbody radius staying constant for a while is a necessary but not a sufficient condition for the presence of tail oscillations in 4U 1636–53.

Both positive and negative drift of the frequency of burst oscillations have been detected in 4U 1636–53 (Strohmayer et al. 1998; Strohmayer 1999). Strohmayer (1999) found that in 4U 1636–53 an episode of a negative frequency drift was correlated with the appearance in the burst of an extended tail of emission with a decay timescale much longer than in other bursts from this source. If we assume that tail oscillations are from vortices in the neutron-star atmosphere (Spitkovsky et al. 2002), the direction in which the vortices drift on the surface of the neutron-star may affect the oscillation frequency. When the vortices move toward the pole, the frequency of oscillations decreases and the low-speed cooling wake makes this a burst with an extended emission tail. When the vortices move toward the equator, the frequency of oscillations increases and the high-speed cooling wake makes these bursts decay fast.

Our analysis shows that tail oscillations in type-I X-ray bursts in 4U 1636–53 are always associated with an emitting area that remains more or less constant for at least $\sim 2 - 8$ s. A similar trend is apparent in another LMXB system, 4U 1728–34 (Zhang et al. in prep.). In hindsight, this trend in 4U 1728–34 is already visible in Fig. 1 of van Straaten et al. (2001) and in 4U 1731–260 in Fig. 5 of Munro et al. (2000), although it was then not recognized by those authors, probably because of the low number of bursts available at the time.

ACKNOWLEDGMENTS

This research has made use of data obtained from the High Energy Astrophysics Science Archive Research Center (HEASARC), provided by NASA’s Goddard Space Flight Center. We thank Laurens Keek, Rudy Wijnands, Chris Done, Peter Jonker, Diego Altamirano, and Anna Watts for useful comments and discussions. TMB acknowledges support from INAF/ASI grant I/009/10/0.

REFERENCES

- Arnaud K. A., 1996, in G. H. Jacoby & J. Barnes ed., *Astronomical Data Analysis Software and Systems V* Vol. 101 of *Astronomical Society of the Pacific Conference Series*, XSPEC: The First Ten Years. p. 17
- Basinska E. M., Lewin W. H. G., Sztajno M., Cominsky L. R., Marshall F. J., 1984, *ApJ*, 281, 337
- Belloni T., Hasinger G., 1990, *A&A*, 230, 103
- Berger M., van der Klis M., van Paradijs J., Lewin W. H. G., Lamb F., Vaughan B., Kuulkers E., Augusteijn

- T., Zhang W., Marshall F. E., Swank J. H., Lapidus I., Lochner J. C., Strohmayer T. E., 1996, *ApJ*, 469, L13
- Bildsten L., 1995, *ApJ*, 438, 852
- Chakrabarty D., Morgan E. H., Muno M. P., Galloway D. K., Wijnands R., van der Klis M., Markwardt C. B., 2003, *Nature*, 424, 42
- Cooper R. L., Narayan R., 2007, *ApJ*, 657, L29
- Cumming A., 2005, *ApJ*, 630, 441
- Cumming A., Bildsten L., 2000, *ApJ*, 544, 453
- Cumming A., Morsink S. M., Bildsten L., Friedman J. L., Holz D. E., 2002, *ApJ*, 564, 343
- Franco L. M., 2001, *ApJ*, 554, 340
- Galloway D. K., Chakrabarty D., Muno M. P., Savov P., 2001, *ApJ*, 549, L85
- Galloway D. K., Muno M. P., Hartman J. M., Psaltis D., Chakrabarty D., 2008, *ApJS*, 179, 360
- Groth E. J., 1975, *ApJS*, 29, 285
- Hasinger G., van der Klis M., 1989, *A&A*, 225, 79
- Heyl J. S., 2004, *ApJ*, 600, 939
- Kapteijn R. G., in't Zand J. J. M., Kuulkers E., Verbunt F., Heise J., Cornelisse R., 2000, *A&A*, 358, L71
- Kuulkers E., Homan J., van der Klis M., Lewin W. H. G., Méndez M., 2002, *A&A*, 382, L947
- Leahy D. A., Darbro W., Elsner R. F., Weisskopf M. C., Kahn S., Sutherland P. G., Grindlay J. E., 1983, *ApJ*, 266, 160
- Lewin W. H. G., van Paradijs J., Taam R. E., 1993, *Space Sci. Rev.*, 62, 223
- Méndez M., van der Klis M., Ford E. C., Wijnands R., van Paradijs J., 1999, *ApJ*, 511, L49
- Muno M. P., 2004, in P. Kaaret, F. K. Lamb, & J. H. Swank ed., *X-ray Timing 2003: Rossi and Beyond Vol. 714 of American Institute of Physics Conference Series, Millisecond Oscillations During Thermonuclear X-ray Bursts*. pp 239–244
- Muno M. P., Chakrabarty D., Galloway D. K., Savov P., 2001, *ApJ*, 553, L157
- Muno M. P., Fox D. W., Morgan E. H., Bildsten L., 2000, *ApJ*, 542, 1016
- Muno M. P., Özel F., Chakrabarty D., 2002, *ApJ*, 581, 550
- Pandel D., Kaaret P., Corbel S., 2008, *ApJ*, 688, 1288
- Payne D. J. B., Melatos A., 2006, *ApJ*, 652, 597
- Piro A. L., Bildsten L., 2005, *ApJ*, 629, 438
- Spitkovsky A., Levin Y., Ushomirsky G., 2002, *ApJ*, 566, 1018
- Strohmayer T., Bildsten L., 2003, *ArXiv Astrophysics e-prints*
- Strohmayer T. E., 1999, *ApJ*, 523, L51
- Strohmayer T. E., Zhang W., Swank J. H., Lapidus I., 1998, *ApJ*, 503, L147
- Strohmayer T. E., Zhang W., Swank J. H., 1997, *ApJ*, 487, L77
- Strohmayer T. E., Zhang W., Swank J. H., Smale A., Titarchuk L., Day C., Lee U., 1996, *ApJ*, 469, L9
- Suleimanov V., Poutanen J., Werner K., 2011, *A&A*, 527, A139
- van Paradijs J., Lewin H. G., 1986, *A&A*, 157, L10
- van Straaten S., van der Klis M., Kuulkers E., Méndez M., 2001, *ApJ*, 551, 907
- Vaughan B. A., van der Klis M., Wood K. S., Norris J. P., Hertz P., Michelson P. F., van Paradijs J., Lewin W. H. G., Mitsuda K., Penninx W., 1994, *ApJ*, 435, 362
- Watts A. L., 2012, *ArXiv e-prints* 1203.2065
- Watts A. L., Strohmayer T. E., Markwardt C. B., 2005, *ApJ*, 634, 547
- Wijnands R., 2001, *ApJ*, 554, L59
- Zhang G., Méndez M., Altamirano D., 2011, *MNRAS*, 413, 1913